photonics

MDPI

Article

RF Injection of THz QCL Combs at 80 K Emitting over 700 GHz Spectral Bandwidth

Andres Forrer, Lorenzo Bosco, Mattias Beck, Jérôme Faist and Giacomo Scalari *

Institute for Quantum Electronics, Department of Physics, ETH Zürich, 8093 Zürich, Switzerland; aforrer@phys.ethz.ch (A.F.); lbosco@phys.ethz.ch (L.B.); mattias.beck@phys.ethz.ch (M.B.); jfaist@ethz.ch (J.F.)
* Correspondence: scalari@phys.ethz.ch

Received: 3 December 2019; Accepted: 14 January 2020; Published: 16 January 2020

Abstract: We report about RF injection locking of an homogeneous THz quantum cascade laser operating at 3 THz central frequency. The extremely diagonal nature of the optical transition, combined with low-loss copper-based double-metal waveguides, allow CW operation up to 105 K and CW power in excess of 5.6 mW measured at 80 K. Terahertz emission spanning up to 600 GHz, together with a narrow beatnote, indicate comb operation at 80 K, and strong RF injection clearly modifies the laser spectrum up to 700 GHz spectral bandwidth making these devices ideal candidates for an on-chip dual comb spectrometer.

Keywords: THz QCL; frequency comb; RF injection; broadband

1. Introduction

Frequency combs have had a tremendous impact in several domains since their demonstration in the early 2000s [1,2]. High-precision spectroscopy [3] and especially dual comb spectroscopy [4] have greatly benefited from the advancement of such sources. The extension of this concept to the different regions of the electromagnetic spectrum has often involved non-linear techniques starting from an ultrafast mode-locked laser operating in the visible or near-infrared. The understanding that sources with perfectly equidistant modes and a well-defined phase relation can be achieved even without ultrafast pulses opened the door to the extension of frequency combs to the mid-IR and THz through optically pumped microresonators [5] and electrically pumped quantum cascade lasers [6,7].

Mid-IR and THz spectral regions are especially important in the fields of sensing and spectroscopy since many chemical species have strong absorption lines there. Such developments gave large momentum to the effort of integrating comb-based spectroscopy platforms onto chip-sized platforms [8]. Quantum cascade lasers [9] are intrinsically well suited to be applied for on-chip integration and a rapid development of QCL-based comb sources has been observed in the past few years. THz QCLs have been shown both to emit ultrashort pulses via active mode locking [10,11] and/or RF switching techniques [12] and also to present wide spectral bandwidth coverage [13–15] in comb emission without pulses [16,17]. Comb operation can be controlled with dispersion compensation [7,18,19] and/or with efficient RF injection locking to metrological sources [20,21].

The requirements for having a robust comb operation are as follows. A wide spectral bandwidth active region that has to feature a reasonably low threshold current density to ease continuous wave (CW) operation over the whole dynamic range, a low-loss waveguide with eventual dispersion [7] and mode control to have only longitudinal modes excited during operation [12].

In this paper, we report on recent advances for producing high-power THz QCL-based combs operating above the technologically important barrier of liquid nitrogen, T = 77 K. In order to improve the performance of our laser ridges, in the present study (for comb generation), we employ low-loss Cu–Cu metal waveguides following the procedure described in Ref. [22], where they were

used in combination with a high-gain two-quantum well structure to increased the maximum operating temperature of THz QCLs up to 210 K. We investigate pulsed and CW output power, their temperature performance and the coherence of comb generation at a temperature of 80 K of such Cu–Cu devices. Further, the comb state is stabilized by RF injection locking and even extended under strong RF injection.

2. Results

The active region employed is a four-quantum-well super-diagonal structure that features a low threshold current density (J_{thresh} = 103 Acm^{-2} resp. J_{thresh} = 157 Acm^{-2} in CW at 20 K resp. 80 K), a wide gain bandwidth and a strong photon driven transport, indication of a long upper state lifetime [23]. The presented active region is fabricated into double-metal ridge waveguides, defined by Inductively Coupled Plasma (ICP) dry-etching, cleaved to the desired cavity length and indium soldered to a copper submount.

Figure 1a shows LIV measurements of a 4 mm long and 86 µm wide double-metal (Cu–Cu) laser ridge as a function of the heat sink temperature both in pulsed and CW operation. Pulsed operation is observed up to 138 K while CW operation stops at 96 K for devices exhibiting a side-absorber with nickel (side-absorber: setback of the top contact on both sides with evaporated nickel. Nickel can be applied during the fabrication process or later on mounted devices. The absorbers have been shown to be instrumental for achieving regular mode spacing in double-metal THz QCLs [12]). Such values are found consistently higher than what is measured on the same epilayer employing Au–Au waveguides. The same device, before having nickel evaporated, even showed CW operation up to 105 K with a threshold current density of 263 Acm^{-2} with the corresponding spectrum shown in the inset of Figure 1b. The pulsed THz power is detected by the Absolut THz Power Meter by *Thomas Keating Ltd* (TK) and in CW by the 3A-P-THz by *Ophir*. The large size TK detector allows direct detection of the unfocused beam in front of the cryostat, whereas the beam for CW detection is focused via two off-axis 90° parabolic mirrors (2″ diam., f/1). The CW powers are then corrected to collection losses of the mirrors and atmospheric absorption. Pulsed peak power and CW peak power are very similar, showing a weak temperature dependence up to 70 K with values close to 8 mW. At 80 K, we still measure 5.6 mW in CW at rollover. The output power of the Cu–Cu lasers is also considerably increased with respect to the Au–Au waveguides (data not shown) [23] at temperatures above 70 K.

In Figure 1b, we compare the temperature dependence of the threshold current density both in pulsed and CW between Au–Au and Cu–Cu waveguides. The impact of the low-loss Cu-based waveguide is clear, yielding an increase of T_{max} of 35 K in pulsed operation and of 10 K in CW. It has to be mentioned that the comparison is not entirely rigorous since the length of the devices are different, i.e., 1.45 mm resp. 4 mm for Au–Au resp. Cu–Cu device , although they have nearly the same width (65 µm resp. 64 µm). Additionally, the temperature dependence of the threshold current can be fitted to $J_{th}(t) = J_0 \cdot exp[T/T_0]$ (in log-scale a line: only temperatures above 70 K for each measurements were considered). T_0 allows to compare different devices and are listed in Figure 1b. The increased T_0 for the Cu–Cu device compared to the Au–Au device in CW indicates an improved temperature performance.

Inspecting the I-V curve, we can note a very strong photon-driven transport yielding a dynamic range that extends with temperature. This is the consequence of the low-loss waveguide combined with a diagonal active region. The maximum current flowing in the structure under laser action depends on the upper state lifetime ($J \propto \frac{1}{\tau_{up}}$) and on the optical field inside the cavity [24,25]. When the temperature increases, the upper state lifetime decreases and the dynamic range is extended since the threshold does not move significantly up to 60 K.

The spectral emission of the same Cu–Cu laser as in Figure 1b at T = 80 K is reported in Figure 2: broadband emission covering over 600 GHz and spectral indication of harmonic states [26,27] are observed. Consistently, the appearance of strong and widely spaced modes with weaker modes in between is observed as it is, for example, very pronounced at 555 mA or 690 mA in Figure 2.

The presented spectra reflect different states in the beatnote map, i.e., high-phase noise, single or multi beatnote regime, shown in Figure 3 at T = 80 K and are discussed in the next paragraph.

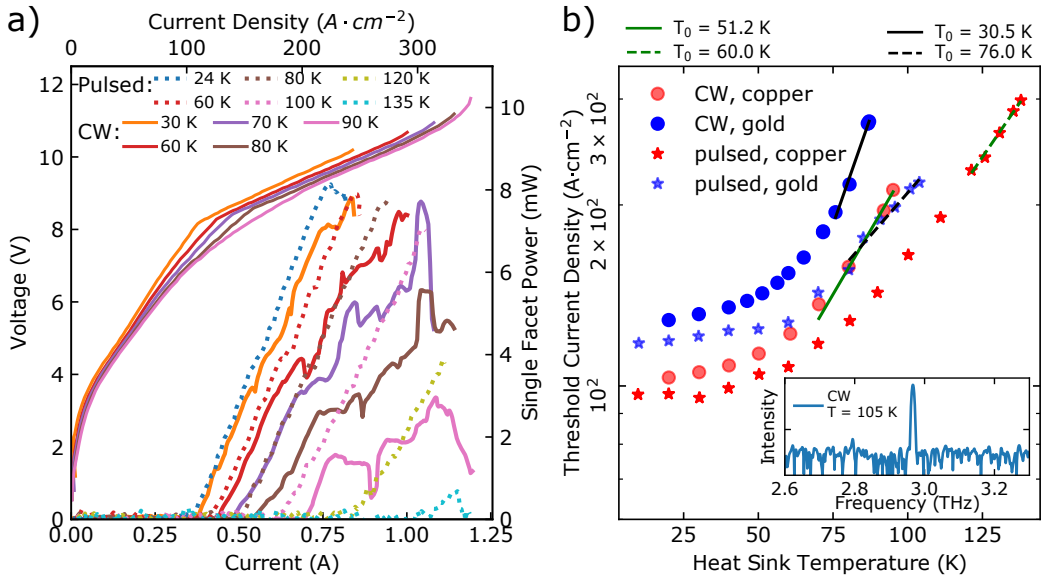

Figure 1. (**a**) LIV Pulsed (2 % duty cycle at 132 kHz repetition rate) and CW of a 4 mm long and 86 µm wide device. For visibility, only CW IV curves are presented. Pulsed power is detected by the Absolut THz Power Meter by *Thomas Keating Ltd* and in CW by the 3A-P-THz by *Ophir*. CW power is corrected for collection losses and atmospheric absorption in the setup to be compared with the pulsed measurements. (**b**) Threshold Current Density vs Temperature of a 4 mm long and 64 µm wide Cu–Cu device and a 1.45 mm long and 65 µm wide Au-Au device. Inset: Increased CW performance of the same Cu–Cu device up to 105 K before having nickel evaporated on the top contact setback, i.e., having side-absorbers.

We then probe the coherence properties of the lasers by recording the electrically detected intermode beatnote as a function of the injected current for different temperatures. In this case, the laser cavity is the same 4 mm long and 64 µm wide Cu–Cu device as in Figure 1b. No intentional dispersion compensation schemes are implemented. The device is mounted infront of the focused FTIR port with a polytetrafluoroethylene (PTFE, teflon) slab (transmission of ~70%) in between to prevent saturation of the internal detector; this also reduces the feedback. The observed effect of feedback only results in constant shifting/jitter of the beatnote frequency (self-mixing effect [28]) in the kHz range due to the constant mirror movement, but not in broadening or destabilisation. This is the configuration for all the following measurements. The CW power at 20 K resp 80 K at rollover is 5.2 mW resp 4.0 mW for this device. As the lasers are operating in CW above 70 K, we can investigate high-temperature coherence behaviour and from the data reported in Figure 3, we can see that a well defined beatnote at the roundtrip frequency is present up to 80 K and even above (not shown). We observe that, in fact, the regions of current where only one well defined beatnote is present, indicated by the pink boxes on the left side of each beatnote map, are more extended as the temperature is increased. Such behaviour is significantly different from what is observed with devices from the same epilayer processed as Au–Au ridges [23].

A possible explanation of this phenomenon is the increased optical field inside the laser cavity combined with the fairly low repetition rate of the investigated devices. The fundamental quantity entering the master equation describing the mode coupling in multimode lasers (i.e., QCLs) is the Rabi frequency written as $\Omega_R = |E_{cav}|d/\hbar$ where d is the electrical dipole of the intersubband laser transition [26,29] and $|E_{cav}|$ the electric field amplitude. If the internal optical field $|E_{cav}|$ is high the peak of the non-linear parametric gain is detuned by $\Omega_R/2$ and then, for low repetition rates, is not

directly favoring four-wave mixing-induced proliferation of nearest neighbour Fabry–Perot modes. The fact that we often observe the high-phase noise instead of the harmonic state indicates that there must be additional parameters influencing the locking mechanism. Other factors to be taken into account are the relatively long upper state life time of the laser (surely longer than 40 ps [30] measured in our previous, less diagonal design), which would result in an intermediate behaviour between AM and FM comb regimes, and the spatial hole burning [31]. The latter is probably reduced for lower temperatures due the particular photon-driven transport in these devices, which leads to a low differential conductance even though the low-loss subwavelength waveguides leads to higher fields.

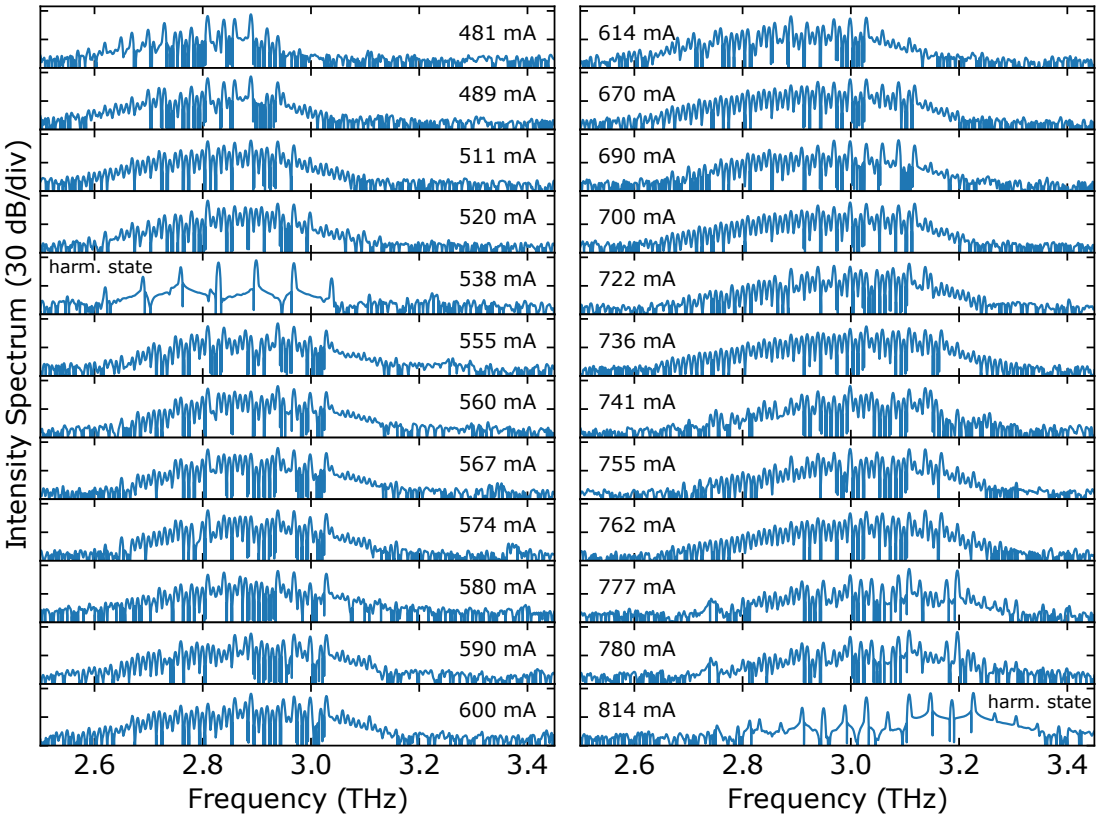

Figure 2. Spectra of a 4 mm long and 64 µm wide device as a function of increasing injected currents at 80 K in CW.

We can further control the coherence of the QCL by means of RF injection locking [32]. Figure 4a shows the injection locking map when the external RF synthesizer frequency is tuned through the repetition rate. As we generally mount chips containing two laser ridges, the synthesizer RF output power of -10 dBm is injected through the neighbouring (unbiased) laser used as an antenna, and the beatnote is measured directly on the laser bias line through a high-frequency bias-tee. The characteristic side modes as well as pulling towards the injection signal and the final locking are observed. Figure 4b shows a free running and injected spectrum. The injected spectrum shows a marginal change for the low injection power. In Figure 4c, we present the narrow (<2 kHz) free running beatnote as well as the lower frequency components. The beatnote has a signal-to-noise of 50 dB and, by injection, we retrieve the same noise floor at low frequencies. Unchanged low-frequency components indicate that, by injection, no destabilization of the comb state occurs. Signals around 2.4 GHz come from the pick up of WiFi signals and below 1 GHz are spurious signals also observed below the lasing threshold. We note that weak injection locking should not change the underlying comb state and only stabilize it, as already observed in Ref. [33].

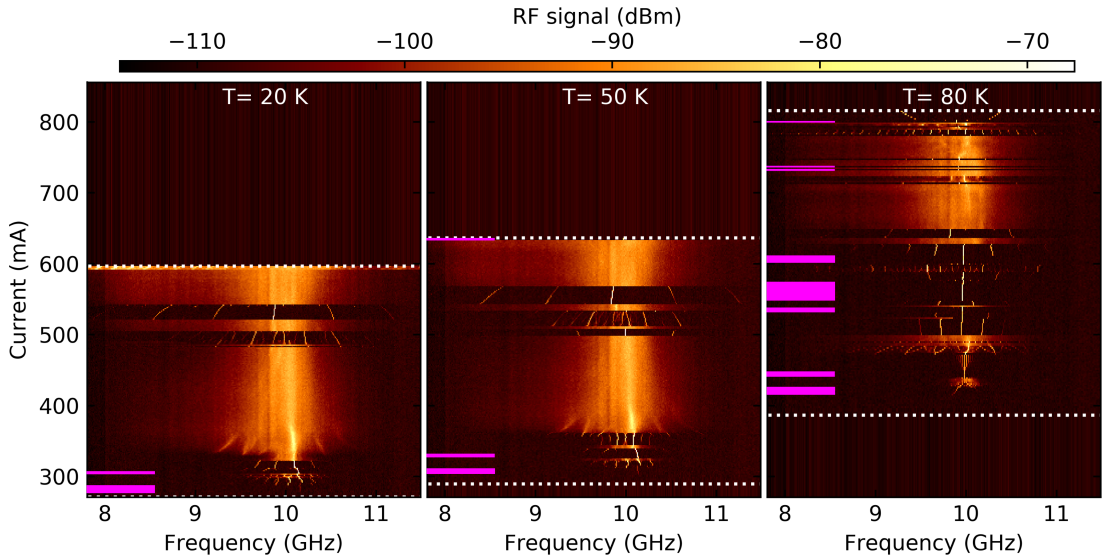

Figure 3. Beatnote maps at 20 K, 50 K and 80 K of the 4 mm long and 64 µm wide copper device. White dotted line indicates the lasing region and the pink blocks indicate regions with a single narrow beatnote around 9.9 GHz.

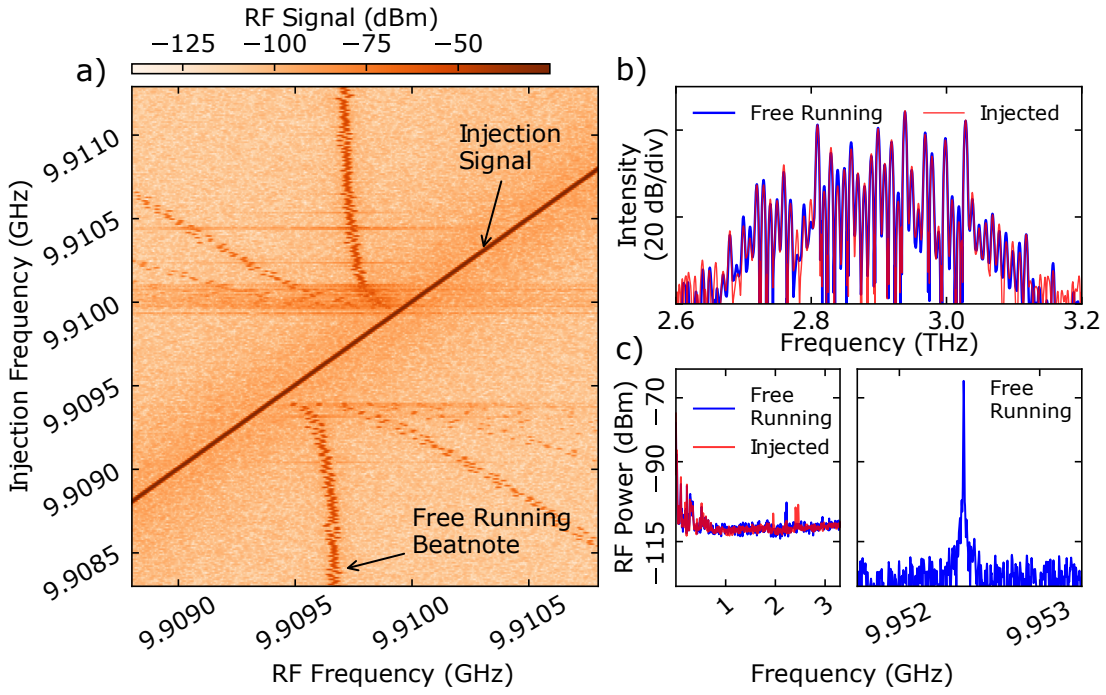

Figure 4. (**a**) Low power (−10 dBm at synthesizer) injection map at 80 K (714 mA, 9.69 V). Injection is via a neighbouring laser acting as an antenna without bias applied. (**b**) Spectra of the free running and injected laser at 80 K (590 mA, 9.12 V). Minor changes due to injection are observed in the spectrum. (**c**) Low-frequency components and narrow (<2 kHz) free running BN at 80K corresponding to the spectra in (**b**). Low-frequency components are unchanged and suggest that injection is not destabilizing the comb state.

In a successive series of measurements, the RF injection via the neighbouring laser is replaced by direct injection on the bias line and observing the beatnote via the neighbouring laser as an antenna. Using a bias-tee this change is done under operation where the laser shows a clear single and narrow beatnote which is then picked up by the neighbouring ridge (with no bias applied) with a reduced

intensity. By the direct injection on the bias line an increased modulation can be achieved which results together with an increased synthesizer injection power of 30 dBm in a broadening of the spectra as shown in Figure 5a. Under RF injection the missing modes are excited and the spectral coverage reaches more than 700 GHz. The nominal FTIR resolution of 2.25 GHz is unable to prove the coherence. Nevertheless, by interpolating, i.e., zero-padding before performing the FFT, the peak position of each mode can be extrapolated. Therefore, Figure 5b presents the mode spacing extracted from the intensity spectrum in Figure 5a which agree well with the free running beatnote and injected frequency. A full proof of the coherence between all modes would need intermode beatnote spectroscopy [6] or SWIFT [7] measurements which would require a sufficient fast THz detector. SWIFT measurements would additionally reveal information of the FM and AM type of the comb emission. Measurements from mid-IR QCL suggest that by strong injection the naturally FM and AM comb regime goes into an AM comb regime, i.e., pulses [33,34]. These findings would also indicate that weak injection preserves the underlying comb state whereas strong injection fundamentally changes the operating state.

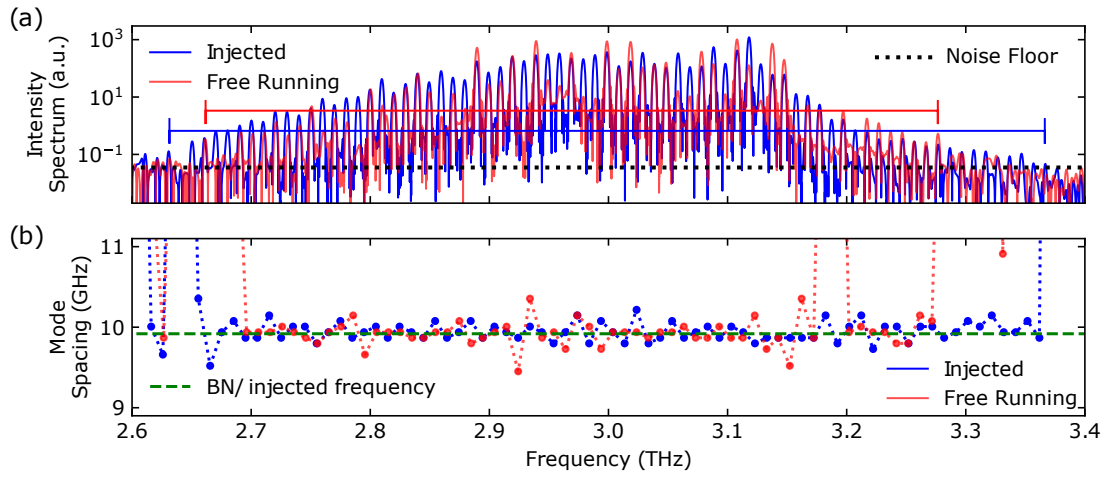

Figure 5. (**a**) Free running (single beatnote regime, 714 mA) and corresponding strong injected spectra at 80 K. Significant change in the modes as well as generation of additional modes due to injection which leads to a spectral bandwidth from 600 GHz to 700 GHz. (**b**) Mode spacing extracted from (**a**) showing a quantitative agreement of the equally spaced modes.

3. Conclusions

We showed the impacts of low-loss Cu–Cu waveguides on laser performance, allowing pulsed operation above 135 K and CW above 95 K, more than 30 K resp 10 K higher than the respective Au–Au counterparts [23]. Simultaneously, output power of roughly 8 mW in pulsed and CW up to 70 K and 5.8 mW in CW at 80 K for a 4 mm long and 85 µm wide device are found. Further, free running comb operation and its injection locking at a temperature of 80 K are demonstrated. By strong injection, the underlying comb state at 80 K is significantly changed, resulting in an increased emission width from 600 to 700 GHz and change in the individual mode intensities. The demonstration of a stable, RF-injected comb at 80 K is significant in view of the application of such devices in dual comb experiments and setups [35,36].

Author Contributions: The active region was designed by G.S. The active region structure was grown by M.B., A.F. and L.B. fabricated the QCL devices. Measurements and data analysis were performed by A.F. and G.S. The project was supervised by J.F. and G.S. All authors have read and agreed to the published version of the manuscript.

Funding: This research was funded by H2020 European Research Council Consolidator Grant (724344) (CHIC) and Schweizerischer National- fonds zur Förderung der Wissenschaftlichen Forschung (200020-165639).

Acknowledgments: The Authors acknowledge discussions with Stefano Barbieri and Philipp Täschler and technical help from Urban Senica.

Conflicts of Interest: The authors declare no conflict of interest.

References

1. Holzwarth, R.; Udem, T.; Hansch, T.; Knight, J.; Wadsworth, W.; Russell, P. Optical frequency synthesizer for precision spectroscopy. *Phys. Rev. Lett.* **2000**, *85*, 2264–2267. [CrossRef]
2. Udem, T.; Holzwarth, R.; Hansch, T. Optical frequency metrology. *Nature* **2002**, *416*, 233–237. [CrossRef]
3. Reichert, J.; Holzwarth, R.; Udem, T.; Hansch, T. Measuring the frequency of light with mode-locked lasers. *Opt. Commun.* **1999**, *172*, 59–68. [CrossRef]
4. Coddington, I.; Newbury, N.; Swann, W. Dual-comb spectroscopy. *Optica* **2016**, *3*, 414–426. [CrossRef]
5. Kippenberg, T.J.; Holzwarth, R.; Diddams, S.A. Microresonator-Based Optical Frequency Combs. *Science* **2011**, *332*, 555–559. [CrossRef] [PubMed]
6. Hugi, A.; Villares, G.; Blaser, S.; Liu, H.C.; Faist, J. Mid-infrared frequency comb based on a quantum cascade laser. *Nature* **2012**, *492*, 229–233. [CrossRef] [PubMed]
7. Burghoff, D.; Kao, T.Y.; Han, N.; Chan, C.W.I.; Cai, X.; Yang, Y.; Hayton, D.J.; Gao, J.R.; Reno, J.L.; Hu, Q. Terahertz laser frequency combs. *Nat. Photonics* **2014**, *8*, 462–467. [CrossRef]
8. Scalari, G.; Faist, J.; Picqué, N. On-chip mid-infrared and THz frequency combs for spectroscopy. *Appl. Phys. Lett.* **2019**, *114*, 150401, doi:10.1063/1.5097933. [CrossRef]
9. Faist, J.; Capasso, F.; Sivco, D.; Sirtori, C.; Hutchinson, A.; Cho, A. Quantum Cascade Laser. *Science* **1994**, *264*, 553–556. [CrossRef]
10. Barbieri, S.; Ravaro, M.; Gellie, P.; Santarelli, G.; Manquest, C.; Sirtori, C.; Khanna, S.P.; Linfield, E.H.; Davies, A.G. Coherent sampling of active mode-locked terahertz quantum cascade lasers and frequency synthesis (vol 5, pg 306, 2011). *Nat. Photonics* **2011**, *5*, 378.
11. Wang, F.; Maussang, K.; Moumdji, S.; Colombelli, R.; Freeman, J.R.; Kundu, I.; Li, L.; Linfield, E.H.; Davies, A.G.; Mangeney, J.; et al. Generating ultrafast pulses of light from quantum cascade lasers. *Optica* **2015**, *2*, 944–949. [CrossRef]
12. Bachmann, D.; Roesch, M.; Süess, M.J.; Beck, M.; Unterrainer, K.; Darmo, J.; Faist, J.; Scalari, G. Short pulse generation and mode control of broadband terahertz quantum cascade lasers. *Optica* **2016**, *3*, 1087–1094. [CrossRef]
13. Forrer, A.; Roesch, M.; Singleton, M.; Beck, M.; Faist, J.; Scalari, G. Coexisting frequency combs spaced by an octave in a monolithic quantum cascade laser. *Opt. Express* **2018**, *26*, 23167–23177. [CrossRef]
14. Roesch, M.; Beck, M.; Süess Martin, J.; Bachmann, D.; Unterrainer, K.; Faist, J.; Scalari, G. Heterogeneous terahertz quantum cascade lasers exceeding 1.9 THz spectral bandwidth and featuring dual comb operation. *Nanophotonics* **2018**, *7*, 237. [CrossRef]
15. Roesch, M.; Scalari, G.; Beck, M.; Faist, J. Octave-spanning semiconductor laser. *Nat. Photonics* **2014**, *9*, 42. [CrossRef]
16. Cappelli, F.; Consolino, L.; Campo, G.; Galli, I.; Mazzotti, D.; Campa, A.; de Cumis, M.S.; Pastor, P.C.; Eramo, R.; Rosch, M.; et al. Retrieval of phase relation and emission profile of quantum cascade laser frequency combs. *Nat. Photonics* **2019**, *13*. [CrossRef]
17. Benea-Chelmus, I.C.; Rösch, M.; Scalari, G.; Beck, M.; Faist, J. Intensity autocorrelation measurements of frequency combs in the terahertz range. *Phys. Rev. A* **2017**, *96*, 033821. [CrossRef]
18. Mezzapesa, F.P.; Pistore, V.; Garrasi, K.; Li, L.; Davies, A.G.; Linfield, E.H.; Dhillon, S.; Vitiello, M.S. Tunable and compact dispersion compensation of broadband THz quantum cascade laser frequency combs. *Opt. Express* **2019**, *27*, 20231–20240. [CrossRef]
19. Wang, F.; Nong, H.; Fobbe, T.; Pistore, V.; Houver, S.; Markmann, S.; Jukam, N.; Amanti, M.; Sirtori, C.; Moumdji, S.; et al. Short Terahertz Pulse Generation from a Dispersion Compensated Modelocked Semiconductor Laser. *Laser Photonics Rev.* **2017**, *11*, 1700013. [CrossRef]
20. Consolino, L.; Nafa, M.; Cappelli, F.; Garrasi, K.; Mezzapesa, F.P.; Li, L.; Davies, A.G.; Linfield, E.H.; Vitiello, M.S.; De Natale, P.; et al. Fully phase-stabilized quantum cascade laser frequency comb. *Nat. Commun.* **2019**, *10*. [CrossRef]
21. Freeman, J.R.; Ponnampalam, L.; Shams, H.; Mohandas, R.A.; Renaud, C.C.; Dean, P.; Li, L.; Davies, A.G.; Seeds, A.J.; Linfield, E.H. Injection locking of a terahertz quantum cascade laser to a telecommunications wavelength frequency comb. *Optica* **2017**, *4*, 1059–1064. [CrossRef]
22. Bosco, L.; Franckié, M.; Scalari, G.; Beck, M.; Wacker, A.; Faist, J. Thermoelectrically cooled THz quantum cascade laser operating up to 210 K. *Appl. Phys. Lett.* **2019**, *115*, 010601. [CrossRef]

23. Forrer, A.; Franckié, M.; Stark, D.; Olariu, T.; Beck, M.; Faist, J.; Scalari, G. Photon-driven broadband emission and RF injection locking of THz quantum cascade laser frequency combs. *arXiv* **2019**, arXiv:1912.00890.
24. Scalari, G.; Amanti, M.I.; Walther, C.; Terazzi, R.; Beck, M.; Faist, J. Broadband THz lasing from a photon-phonon quantum cascade structure. *Opt. Express* **2010**, *18*, 8043–8052. [CrossRef] [PubMed]
25. Scalari, G.; Terazzi, R.; Giovannini, M.; Hoyler, N.; Faist, J. Population inversion by resonant tunneling in quantum wells. *Appl. Phys. Lett.* **2007**, *91*, 032103. [CrossRef]
26. Piccardo, M.; Chevalier, P.; Mansuripur, T.S.; Kazakov, D.; Wang, Y.; Rubin, N.A.; Meadowcroft, L.; Belyanin, A.; Capasso, F. The harmonic state of quantum cascade lasers: Origin, control, and prospective applications (Invited). *Opt. Express* **2018**, *26*, 9464–9483. [CrossRef]
27. Mansuripur, T.S.; Vernet, C.; Chevalier, P.; Aoust, G.; Schwarz, B.; Xie, F.; Caneau, C.; Lascola, K.; Zah, C.e.; Caffey, D.P.; et al. Single-mode instability in standing-wave lasers: The quantum cascade laser as a self-pumped parametric oscillator. *Phys. Rev. A* **2016**, *94*, 063807. [CrossRef]
28. Wienold, M.; Röben, B.; Schrottke, L.; Grahn, H.T. Evidence for frequency comb emission from a Fabry-Pérot terahertz quantum-cascade laser. *Opt. Express* **2014**, *22*, 30410–30424. [CrossRef]
29. Villares, G.; Faist, J. Quantum cascade laser combs: Effects of modulation and dispersion. *Opt. Express* **2015**, *23*, 1651–1669. [CrossRef]
30. G.Derntl, C.; Scalari, G.; Bachmann, D.; Beck, M.; Faist, J.; Unterrainer, K. Gain dynamics in a heterogeneous terahertz quantum cascade laser. *Appl. Phys. Lett.* **2018**, *113*, 81102.
31. Opačak, N.; Schwarz, B. Theory of frequency modulated combs in lasers with spatial hole burning, dispersion and Kerr. *arXiv* **2019**, arXiv:1905.13635.
32. Gellie, P.; Barbieri, S.; Lampin, J.F.; Filloux, P.; Manquest, C.; Sirtori, C.; Sagnes, I.; Khanna, S.P.; Linfield, E.H.; Davies, A.G.; et al. Injection-locking of terahertz quantum cascade lasers up to 35GHz using RF amplitude modulation. *Opt. Express* **2010**, *18*, 20799–20816. [CrossRef]
33. Hillbrand, J.; Beiser, M.; Andrews, A.M.; Detz, H.; Weih, R.; Schade, A.; Höfling, S.; Strasser, G.; Schwarz, B. Picosecond pulses from a mid-infrared interband cascade laser. *Optica* **2019**, *6*, 1334–1337. [CrossRef]
34. Wang, C.Y.; Kuznetsova, L.; Gkortsas, V.M.; Diehl, L.; Kärtner, F.X.; Belkin, M.A.; Belyanin, A.; Li, X.; Ham, D.; Schneider, H.; et al. Mode-locked pulses from mid-infrared Quantum Cascade Lasers. *Opt. Express* **2009**, *17*, 12929–12943. [CrossRef] [PubMed]
35. Yang, Y.; Burghoff, D.; Hayton, D.J.; Gao, J.R.; Reno, J.L.; Hu, Q. Terahertz multiheterodyne spectroscopy using laser frequency combs. *Optica* **2016**, *3*, 499–502. [CrossRef]
36. Sterczewski, L.A.; Westberg, J.; Yang, Y.; Burghoff, D.; Reno, J.; Hu, Q.; Wysocki, G. Terahertz hyperspectral imaging with dual chip-scale combs. *arXiv* **2018**, arXiv:1812.03505.